# The Bandgap as a Moving Target: Reversible Bandgap Instabilities in Multiple-Cation Mixed-Halide Perovskite Solar Cells

*Fabian Ruf[1] *, Pascal Rietz[1], Meltem F. Aygüler[2], Ina Kelz[1], Pablo Docampo[3], Heinz Kalt[1], and Michael Hetterich[1,4] **

[1]Institute of Applied Physics, Karlsruhe Institute of Technology (KIT), Wolfgang-Gaede-Str. 1, 76131 Karlsruhe

[2]Department of Chemistry and Center for NanoScience (CeNS), LMU Munich, Butenandstr. 5-13, 81377 München, Germany

[3]Physics Department, School of Electrical and Electronic Engineering, Newcastle University, Newcastle upon Tyne, NE1 7RU, United Kingdom

[4]Light Technology Institute, Karlsruhe Institute of Technology (KIT), Engesserstr. 13, 76131 Karlsruhe, Germany

**Corresponding Author**

*E-mail: fabian.ruf@kit.edu (FR), michael.hetterich@kit.edu (MH)

**Abstract**

Multiple-cation mixed-halide perovskites show high power-conversion efficiencies and recently improved stability. But, even most advanced absorber materials still suffer from instabilities of the bandgap under illumination and applied bias. Here we employ modulation spectroscopy as a highly sensitive electro-optical measurement technique to directly reveal such instabilities. We find a reversible decrease of the absorber bandgap of up to 70meV in complete solar cells. In-situ X-ray diffraction measurements under illumination and bias confirm structural changes of the perovskite and their reversibility, which are attributed to segregation of the halides. These processes are most strongly activated when combining illumination and bias which leads to a five-times increased shift compared to illumination only. Since this scenario is intrinsic to the solar cell's operation conditions, it can never be avoided completely. Furthermore, the bandgap decrease is strongly enhanced – but still reversible – by high relative humidity and oxygen supporting the strict requirement of efficient encapsulation.

**TOC GRAPHICS**

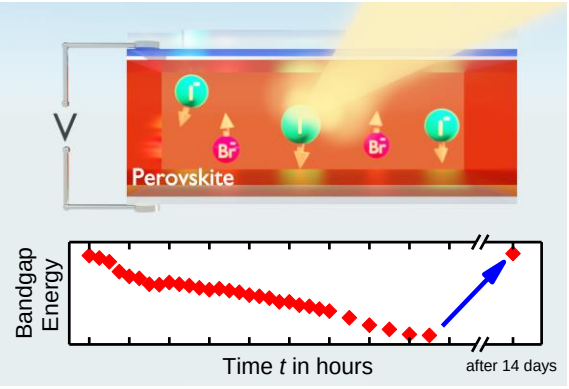

Metal halide perovskites have proven their suitability for a wide range of optoelectronic applications. Most prominent are thin-film photovoltaics due to a high power-conversion efficiency of perovskite-based solar cells exceeding 22%.[1-4] Mixed-halide compounds even offer a tunability of the bandgap energy over a wide range, enabling the integration in tandem cells as well as in lasers and lighting devices.[5-13] Of paramount importance for such applications is the stability of the perovskite under typical operation conditions and indeed significant improvements have been recently reported.[14-15]

But, there are still problems with structural stability of the perovskite absorber due to segregation effects, e.g., light-induced phase segregation into iodide-rich and bromide-rich domains in $MAPb(I_{1-x}Br_x)_3$ leading to a decreased open-circuit voltage and additional recombination paths in iodide-rich domains.[16-19] Multiple-cation mixed-halide perovskites have been found to strongly suppress segregation under illumination and are generally accepted to be structurally more stable.[20,21] However, the impact of macroscopic electric fields, e.g., by an applied voltage, has not been studied in detail.

In this contribution, we want to address compositional changes of perovskite absorber layers by analysis of modulation spectra. Using this technique, we are able to investigate complete thin-film solar cells in a non-destructive way under operation-relevant conditions. The principle of the analysis is based on the fact that segregation of halide ions directly affects the bandgap energy of the absorber layer.[22-24] In particular electroreflectance (ER) spectroscopy is well suited for the precise determination of small energy shifts of critical points in the band structure, such as the bandgap.[24-28] By applying an AC bias to the solar cell and, thereby, periodically modulating the electric field in the absorber layer, the dielectric function $\varepsilon$ is modulated. The dielectric function, in turn, is directly related to measurable optical properties, e.g., the reflectivity $R$. The relative

change $\Delta R$ / $R$ exhibits sharp oscillator features, which enable precise determination of the resonance energy of optical transitions.[23,29-31]

Here, we study a potential phase segregation of iodide and bromide in the multiple-cation mixed-halide perovskite $Cs_{0.05}(FA_{0.83}MA_{0.17})_{0.95}Pb(I_{0.83}Br_{0.17})_3$ (CsFAMA(I,Br)). Band-structure changes, for the first time directly monitored by ER spectroscopy, reveal that these compositional effects are reversible. They are most strongly activated under the combined influence illumination and applied bias (AC or DC) which proves indeed the strong impact of electric fields. Moreover, high relative humidity and oxygen content significantly increase the observed bandgap shifts which are still fully reversible.

For the measurements, we have prepared highly efficient perovskite solar cells in a stack of FTO/$TiO_2$/perovskite/spiro-OMeTAD/Au with different perovskite compositions as can be seen in Figure S1. To study the effects of bandgap instabilities in CsFAMA(I,Br) based solar cells under illumination (~1sun) and additional electric fields (in air), ER spectra were recorded consecutively every 15 minutes with applied AC bias (sinusoidal, amplitude $V_{max} = \pm 0.5$ V, frequency $f = 990$ Hz). necessary for the measurements (see Supporting Information for details). Figure 1 (a) shows the evolution of the ER spectra over a total measurement time of about 8 hours (from green to red curves). Besides a moderate decrease in amplitude, the spectra exhibit a distinct bandgap shift to lower energies. After recovery in the dark without an applied bias, the initial spectrum was restored (dashed blue line) which demonstrates the reversibility of the bandgap energy and the causing compositional changes in the perovskite.

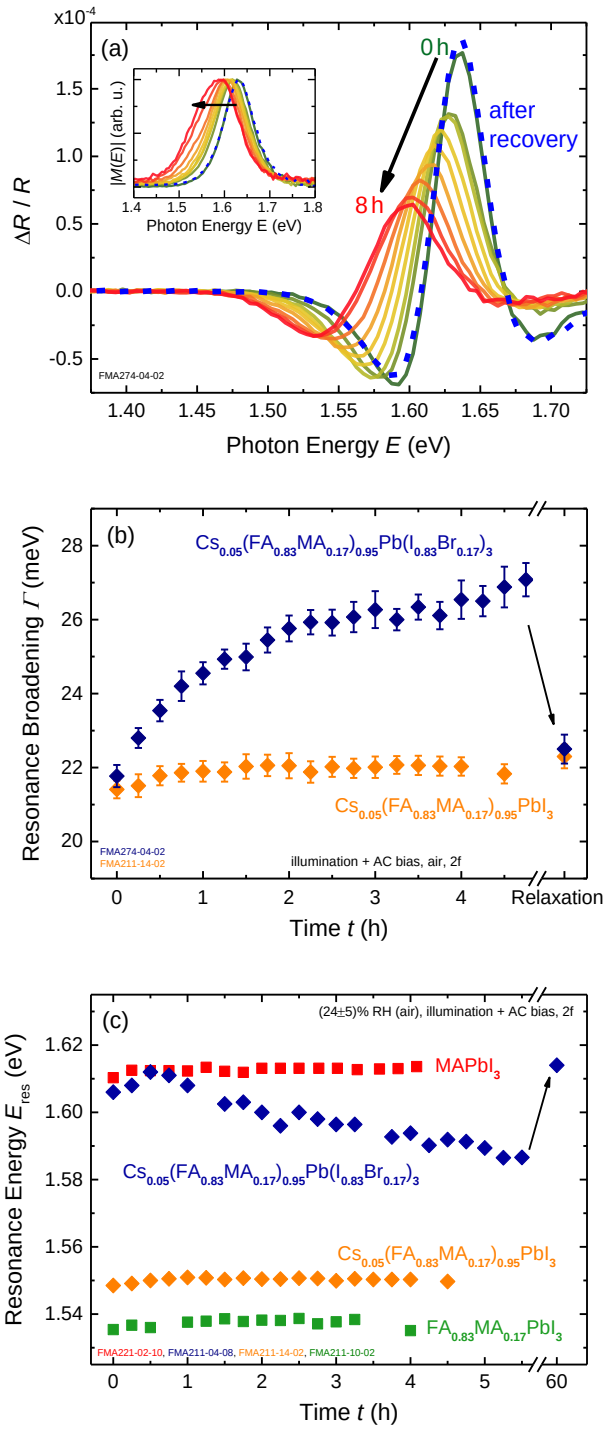


**Figure 1.** Reversible bandgap shifts and resonance broadening of CsFAMA(I,Br). (a) The ER resonance feature shifts to lower energies under illumination and AC bias conditions (green to red curve). The initial spectrum is restored after sufficient recovery in the dark (dashed blue line).

(inset) The corresponding transformed modulus spectra illustrate the shift and broadening of the resonance. (b) The resonance broadening of triple-cation perovskites with and without bromide. An increase of the resonance broadening $\Gamma$ only occurs for mixed-halide compounds. (c) Comparison of the resonance energy under illumination and AC bias of different absorber compositions. Only the CsFAMA(I,Br) compound (blue data points) containing iodide and bromide exhibits a reversible decrease of the resonance energy.

In order to precisely determine the energy of the optical resonance, we transformed the experimentally measured $\Delta R / R$ spectra to so-called modulus spectra utilizing an approach based on Kramers—Kronig relations. The resulting transformed spectra $| M(E) |$ possess a peak-like line shape and facilitate a precise determination of the peak position that is associated with the resonance energy. Further details on the transformation method can be found in references and Supporting Information.[32,33] The inset of Figure 1 (a) depicts the evolution of the normalized transformed $| M(E) |$ (compared to the measured $\Delta R / R$ signal as main graph in Figure 1 (a)) over time, i.e., under continued influence of illumination and bias (from green to red). Additionally to the already discussed shift of the resonance energy to lower values, the spectra reveal a broadening of the peak shape over time, which can be attributed to an increasing inhomogeneity of the perovskite absorber. Furthermore, we want to emphasize that not only the position of the modulus peak but also the width was restored to its initial value after recovery in the dark for several days (dashed blue line). To quantify this behavior, the spectral broadening $\Gamma$ can be determined by directly fitting a so-called "First-Derivative Functional Form" (FDFF) line shape to the experimental ER spectra (see Supporting Information for details). Figure 1 (b) demonstrates the significant increase of $\Gamma$ from ~22 meV up to ~31 meV after 8 hours, but, remarkably, it is

completely restored to its initial value after sufficient recovery in the dark – at the latest after 14 days.

In order to further investigate the influence of different cations of the perovskite absorber and to rule out some of the possible explanations for the observed photo- and voltage-induced bandgap shifts, we fabricated solar cells with different absorber compositions. We successively left out bromide, cesium, and formamidinium ions and measured the bandgap behavior under illumination and AC bias. Figure 1 (c) presents the change of the bandgap energy for the different absorber compositions for about 5 hours measurement time. Here, only the bromide-containing compound, CsFAMA(I,Br) (blue data points), shows a significant change of the resonance energy. Thus, this observation is in good agreement with the hypothesis of a photo- and voltage-induced phase segregation of the halides. We note that for $Cs_{0.05}(FA_{0.83}MA_{0.17})_{0.95}PbI_3$ (CsFAMAI), a small shift to lower energies of about 5 meV was detected under high relative humidity conditions which might be caused by the formation of a Cs-rich secondary phase and was also identified in CsFAMA(I,Br).[34] Apart from these minor effects due to the cesium ions, we did not find any contribution of the cations. This can be explained by the smaller mobility and availability for ion movement compared to halide anions and supports the conclusion of moving halide ions.[35] Accordingly, no change of the spectral broadening $\Gamma$ is found for samples with pure iodide perovskite (see Figure 1 (b)).

**Structural Analysis Using X-Ray Diffraction.** For further clarification of the underlying structural changes, we performed X-ray diffraction (XRD) measurements on CsFAMA(I,Br). In order to directly assess the influence of a continuous illumination and applied bias, we tracked the changes in the X-ray diffractograms in-situ. The comparison of the perovskite peaks at 24.6° and 28.4° in Figure 2 (a) + (b) before (black line) and after illumination and bias (red line) clearly

reveals changes in the peak shape and thereby the crystal structure, especially on the small-angle side of both peaks. The shoulder at lower angles (~ 28.3° in Figure 2 (b)) can be ascribed to the formation of an iodide-rich phase under illumination due to the increased lattice parameter compared to the mixed iodide–bromide phase. On the large-angle side (~ 28.5° in Figure 2 (b)), we observed a smaller shoulder-like feature which indicates a bromide-rich phase formed due to the migration of iodide ions. In good agreement with the ER measurements, the XRD pattern recovered its initial shape nearly completely after 7 days relaxation in the dark (blue curve). From the decrease of the peak height before and after illumination and bias, we estimate the ratio of perovskite segregated into iodide-rich and bromide-rich domains compared to the intermixed phase to be about 25% of the perovskite absorber. Furthermore, we monitored the evolution of the 14.1° perovskite peak under illumination and applied voltage over 5 hours (from green to red in Figure 2 (c)). The (normalized) spectra exhibit a clear asymmetric broadening on the lower-angle side around 14.05°, which can be again attributed to the formation of a dominant iodide-rich phase. To quantify the increased broadening, we show the Full-Width Half-Maximum (FWHM) of the normalized spectra over time in Figure 2 (d). Consistent with the observations described above, the FWHM continuously increases with time due to the advancing segregation of the halides indicating an increasing inhomogeneity of the crystal structure. After termination of the illumination and applied bias, the structural changes are nearly fully reversed after 7 days, which is reflected by the FWHM as well as the diffractograms in Figure 2 (c). In conclusion, the in-situ XRD analysis proves reversible changes in the crystal structure of the CsFAMA(I,Br) perovskite absorber layer under continuous illumination and applied bias and, therefore, confirms the conclusion of a photo- and voltage-activated segregation of the halides.

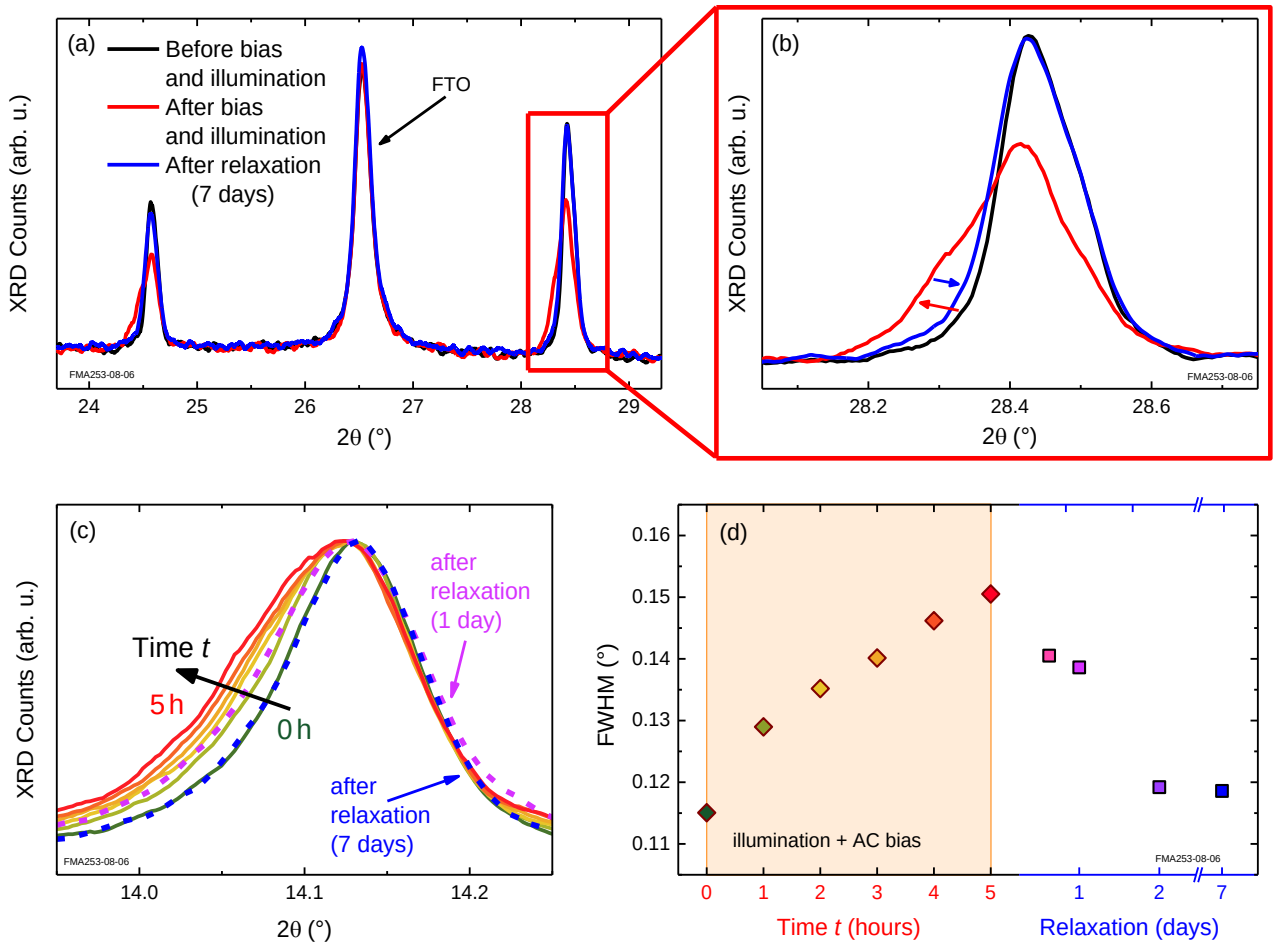


**Figure 2.** Reversible changes in the crystal structure revealed by XRD measurements. (a) XRD spectra of the 24.6° and 28.4° perovskite peaks before (black curve) and after illumination and bias (red curve) as well as after relaxation (blue curve). The XRD reflexes broaden towards lower angles which can be attributed to an iodide-rich phase arising. After 7 days in the dark, the initial spectrum is restored. (b) Enlargement of the 28.4° perovskite reflex. (c) Monitoring of the 14.1° perovskite peak under white-light illumination and AC bias by in-situ XRD measurements. The spectra are normalized with respect to the maximum and exhibit a clear asymmetric broadening towards lower angles over 5 hours of influence (green to red curves). After relaxation in the dark, the peak recovers its initial shape (dashed purple and blue line). (d) Full-Width Half-Maximum of the 14.1° peak in (c). Under illumination and voltage, FWHM is continuously increasing.

Relaxation starts after termination of external activation and nearly restores the initial values after 7 days in the dark.

**Dependence of Illumination and Applied Voltage.** In order to disentangle the impact of illumination and applied bias, we performed measurement series with either a ~1 sun illumination or an applied AC bias (sinusoidal, amplitude $V_{max} = \pm 0.5$ V, frequency $f = 990$ Hz) or the combination of both and compared the average shifts of the bandgap energy (see Figure 3 (a)). For a more distinct assignment of the influencing factors of the observed bandgap shifts, ER spectra were only recorded directly before and after a 4-hour interval of a defined voltage and illumination condition (see Supporting Information for details).

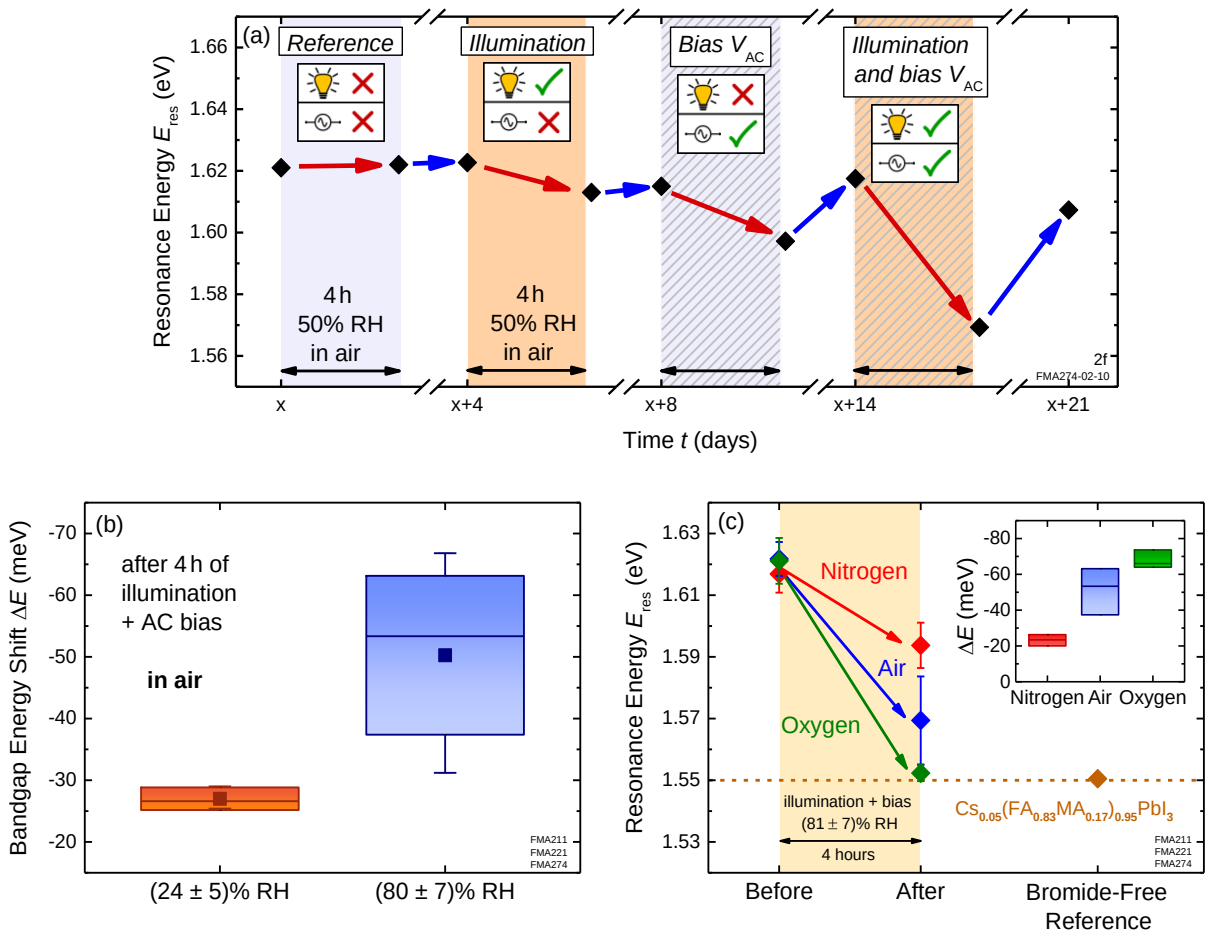


**Figure 3.** Effects of different influencing factors on the shift of the bandgap energy in CsFAMA(I,Br). (a) Separation of the impact of illumination and bias. For the illumination-only or bias-only cases, the sample exhibit only moderate shifts of ~10 meV and ~20 meV, respectively. Under the combined effect of illumination and AC bias, the obtained shifts are strongly increased up to ~50 meV. (b) Bandgap energy shifts in different relative humidity conditions under illumination and bias. In air, the extent of the energy shift is strongly increased from 25–30 meV up to (50 ± 13) meV for high relative humidity. (c) Resonance energy change in different atmospheric conditions under relative humidity of about 80%. The final resonance energy is decreased by increasing oxygen content, starting from similar values. For pure oxygen (green data points), the final energy is close to the resonance of the CsFAMAI compound (orange data point,

for comparison) without any bromide indicating strong halide segregation. (inset) The corresponding values for the bandgap energy shift in nitrogen (red), air (blue) and oxygen (green).

In the illumination-only case, small shifts of the bandgap energy in the order of about 10 meV reflect the expected enhanced compositional stability of the CsFAMA(I,Br) perovskite. In that sense, our results confirm the expected increased robustness against photo-induced halide segregation effects.[19,20] In this context, the spectral dependency of these processes is also an interesting aspect which might be relevant for applications. First results filtering out the UV light did not show a significant influence on the observed bandgap shifts. However, further studies are needed to clarify this in detail. In order to realistically determine the impact of photo-induced halide segregation on the compositional stability under solar-cell relevant conditions not only the illumination of 1 sun is crucial but also the additional effect of electric fields, here by an applied bias. Clearly, the combined application of illumination and voltage affects the perovskite most strongly and leads to the largest bandgap shift of about 50 meV, also exceeding the shift of about 20 meV in the voltage-only case.

Different models have been developed to explain photo-induced halide segregation in mixed perovskites, including thermodynamic reasoning from two minima in the Helmholtz free energy or polaron-assisted cluster formation and stabilization. [19,36-38] Still, an additional electric field can be understood as supporting effect to the driving forces in each of the proposed models – either as additional kinetic activation energy or as additional induced strain. The latter might be an alternative perception of the increasing FWHM of the XRD peaks under illumination and voltage based on increased micro-strain.[20,39] Furthermore, Barker *et al.* proposed a strong gradient in charge-carrier generation due to one-sided illumination in the strongly absorbing perovskite layer

leading to iodide-rich domains mostly close to the illuminated side of the sample via halide defects.[39] Additional applied electric fields could enhance the mobility of the halide defects and, therefore, assist the segregation. Our results emphasize the necessity to include voltage-induced effects into stability considerations of mixed-halide perovskites. Despite the increased robustness against halide segregation in CsFAMA(I,Br) compared to $MAPb(I_xBr_{1-x})_3$, we observed a significant decrease of the bandgap energy, which is detrimental to solar cell performance and cannot be avoided, e.g., by encapsulation of the devices.

**Influence of Atmospheric Conditions.** Under the combined influence of a ~1sun illumination and an applied AC bias, we could detect a decrease of the bandgap energy for all samples with CsFAMA(I,Br) absorber layer. Nevertheless, the extent of the energy shift is strongly dependent on additional atmospheric conditions such as relative humidity (RH) and oxygen content and ranges from approximately 20 meV up to 70 meV. Therefore, we conducted a more detailed study on the relevant influencing factors of the occurring reversible processes under operation-relevant atmospheric conditions (illustrated in Figure S2 (b)). After a sufficient relaxation time, the starting level of the resonance energy before the next measurement is at a comparable value of about 1.62 eV. For a higher relative humidity (80% RH compared to 23% RH), the extent of the bandgap shift is increased from ~30 meV to over 50 meV. However, if the same relative humidity is used but in a nitrogen atmosphere instead of air, the change of the energy is even below 25 meV, indicating a combined effect of both influencing factors. Figure 3 (b) summarizes the results of the observed bandgap changes for high and low relative humidity in air, meaning 24% RH and 80% RH, respectively. In the low-humidity case values range from 25 meV to 30 meV, for a high relative humidity the spread of the obtained values is much larger with an average shift of (50 ± 13) meV. The relatively large range might be attributed to variations of absorber and interface

properties such as morphology or passivation as well as different aging behavior under these conditions. However, the comparative analysis reveals a significant increase of the bandgap shifts under high relative humidity in air. Furthermore, we investigated the effect of the oxygen content in the surrounding atmosphere by changing from air to either nitrogen or pure oxygen. For pure nitrogen, the change of the resonance energy shows itself to be unaffected by the relative humidity with rather low values, ranging from 20 meV up to 30 meV. This could be caused by the overall small shifts under nitrogen atmosphere emphasizing the importance of oxygen for observed effects. For a high relative humidity, the results under different gas atmospheres are summarized in Figure 3 (c). Starting from about the same value of 1.62 eV, the resonance energy shifts to lower values with increasing oxygen content. For pure oxygen (green data points), the bandgap shift exceeds 70 meV and the resonance energy reaches values as low as 1.55 eV after 4 hours of external stimulation by illumination and voltage. Remarkably, these low values are only slightly above the observed resonance energies for CsFAMAI samples (orange data point, for comparison) which do not contain any bromide. This indicates that most of the halides could be driven into segregation under the aforementioned conditions. This conclusion is in good agreement with the fact that we did not observe any value for the resonance energy below 1.55 eV, even under the most extreme conditions, i.e., pure oxygen and high relative humidity.

The strongly increased shift of the bandgap energy for high relative-humidity conditions can be attributed to an increased mobility of the halide ions.[40,41] In the context of a defect-assisted segregation mechanism, an enhanced mobility leads to faster halide segregation and, thus, a stronger shift of the effective resonance energy. Additionally, the formation of a perovskite-monohydrate decreases homogeneity of the perovskite layer and, therefore, might increase strain-induced segregation.[19,34,37,42] The oxygen in the surrounding atmosphere probably leads to the

formation of superoxides under illumination. However, the effect on the reversible changes on the bandgap energy remains unclear since superoxides cause an irreversible degradation of perovskite absorber, which leads to further defects but cannot explain the reversibility.[43,44]

Generally, the strongly reduced bandgap shift in CsFAMA(I,Br) perovskite solar cells under nitrogen and low relative humidity opens up the prospect to reduce these kind of effects by effective encapsulation. This will not completely inhibit the halide segregation under illumination and voltage, as it is intrinsic to the solar cell operation conditions, but could reduce its detrimental effects on solar cell performance.

**Effects Under DC Bias Conditions.** In order to complete our detailed studies of reversible bandgap changes under realistic solar cell conditions, we performed additional measurements under illumination but with a DC instead of an AC voltage of 0.5 V in forward or reverse direction. Figure 4 (a) presents the time evolution of the ER resonance over a total measurement time of 12 hours measured consecutively every 30 minutes under a forward DC bias of 0.5 V. Compared to the continuous shift and broadening of the resonance under applied AC bias (see Figure 1), the modulus spectra and the original ER spectra (see inset) exhibit more severe deformations under DC voltages. After about 6 hours of illumination and applied DC voltage, the intensity of the high-energy peak at 1.63 eV starts to decrease whereas the intensity of the low-energy peak at 1.55 eV increases over time, leading to a strong dominance of the 1.55 eV peak after 12 hours. Figure 4 (b) demonstrates a similar behavior in case of a DC voltage of 0.5 V in reverse bias direction. In that case, ER spectra were obtained only before and after a 4-hour interval of illumination and DC forward bias. The co-existence of both resonances is clearly visible after only 4 hours, even in the non-transformed ER spectra (see inset). We attribute the 1.63 eV to the iodide–bromide intermixed phase and the 1.55 eV to the iodide-rich phase, respectively. The low-energy resonance is again in

very good agreement with the resonance energy of the CsFAMAI perovskite containing no bromide at all. This indicates the formation of domains consisting of virtually pure iodide perovskite. In comparison, in the case of an AC bias, the phase segregation exhibits itself as a continuous bandgap shift over nearly the same energy interval down to 1.55 eV as well as an additional broadening of the ER resonance. This can be understood in terms of an increasing number of small iodide-perovskite domains in the intermixed phase which translates into an 'effective' bandgap of the whole absorber layer. Due to the unidirectional nature of the electric field in the case of an applied DC bias, we hypothesize the formation or accumulation of larger domains close to the front and back contact (due to different mobilities of iodide and bromide) leading to a clearly resolved low-energy resonance.

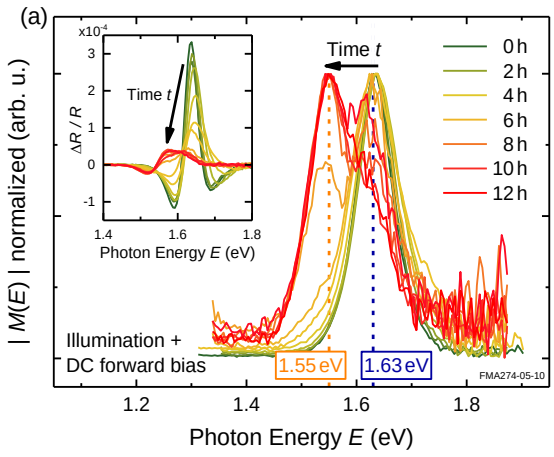

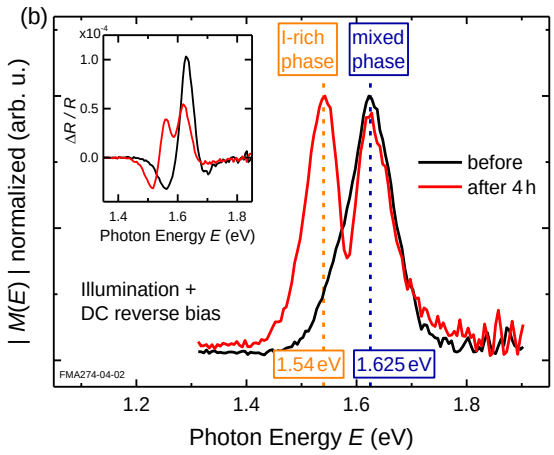


**Figure 4.** Halide segregation effects under DC bias conditions (~1 sun illumination and DC bias of 0.5 V). (a) Under forward bias conditions, the relative amplitude of the initial high-energy resonance at 1.63 eV decreases and a second low-energy resonance at 1.55 eV arises after 8 hours of exposure (green to red curves). (inset) Corresponding deformation effects in the ER spectra. (b) Comparison of the resonance and ER spectra (inset) before (black curve) and after (red curve) 4 hours of illumination and DC reverse bias. The co-existence of a high and low energy resonance at 1.625 eV and 1.54 eV, respectively, is observed similarly to (a). The two peaks are attributed to the intermixed phase of iodide and bromide (dashed blue line) and an iodide-rich phase (dashed orange line) containing virtually no bromide.

In conclusion, by using modulation spectroscopy, we demonstrated that photo- and voltage-induced halide segregation plays a significant role even in CsFAMA(I,Br) perovskites, which are generally considered to be stable against segregation effects. These compositional changes manifest themselves as a decrease of the bandgap energy accompanied by a resonance broadening in the case of an AC bias and are confirmed by in-situ XRD measurements. This can be explained by the formation and accumulation of small iodide-perovskite domains in the intermixed phase.

While the bandgap shifts are small under 1 sun illumination only, we found significantly increased shifts by a factor of 5 with an additionally applied bias. Since illumination and voltage are intrinsic to the cell's operation conditions, these effects cannot be avoided completely. An additional analysis of atmospheric influencing factors shows strong – but still reversible – effects of high relative humidity and oxygen content which confirms the necessity to reduce these detrimental effects by effective encapsulation.

## ASSOCIATED CONTENT

**Supporting Information.** Layer stack and power-conversion efficiencies, experimental details of ER and XRD measurements, modulus transformation and fitting of ER spectra, further confirmation of reversibility, sample preparation and solar cell characterization.

## AUTHOR INFORMATION

**Corresponding Authors**

*E-mail: fabian.ruf@kit.edu (FR); michael.hetterich@kit.edu (MH)

## ACKNOWLEDGMENT

We acknowledge financial support by the German Federal Ministry of Education and Research (BMBF) under the project ID FKZ 03SF0516, and the Karlsruhe School of Optics and Photonics

(KSOP) at KIT. M.F.A. gratefully acknowledges the Scientific and Technological Research Council of Turkey.

REFERENCES

(1) Green, M. A.; Hishikawa, Y.; Dunlop, E. D.; Levi, D. H.; Hohl- Ebinger, J.; Ho- Baillie, A. W. Y. Solar cell efficiency tables (version 52). *Prog Photovolt Res Appl*. **2018**, *26*, 427–436.

(2) Yang, W. S.; Park, B.-W.; Jung, E. H.; Jeon, N. J.; Kim, Y. C.; Lee, D. U.; Shin, S. S.; Seo, J.; Kim, E. K.; Noh, J. H.; *et al.* Iodide Management in Formamidinium-Lead-Halide–Based Perovskite Layers for Efficient Solar Cells. *Science* **2017**, *356*, 1376-1379.

(3) Saliba, M.; Matsui, T.; Domanski, K.; Seo, J.-Y.; Ummadisingu, A.; Zakeeruddin, S. M.; Correa-Baena, J.-P.; Tress, W. R.; Abate, A.; Hagfeldt, A.; *et al.* M. Incorporation of Rubidium Cations into Perovskite Solar Cells Improves Photovoltaic Performance. *Science* **2016**, *354*, 206-209.

(4) Docampo, P.; Ball, J. M.; Darwich, M.; Eperon, G. E.; Snaith, H. J. Efficient Organometal Trihalide Perovskite Planar-Heterojunction Solar Cells on Flexible Polymer Substrates. *Nat. Comm.* **2013**, *4*, 2761.

(5) Wu, Y.; Yan, D.; Peng, J.; Duong, T.; Wan, Y.; Phang, S. P.; Shen, H.; Wu, N.; Barugkin, C.; Fu, X.; *et al.* Monolithic Perovskite/Silicon-Homojunction Tandem Solar Cell with over 22% Efficiency *Energy Environ. Sci* **2017**, *10*, 2472-2479.

(6) Shen, H.; Duong, T.; Peng, J.; Jacobs, D.; Wu, N.; Gong, J.; Wu, Y.; Karuturi, S. K.; Fu, X.; Weber, K.; *et al.* Mechanically-Stacked Perovskite/CIGS Tandem Solar Cells with Efficiency of 23.9% and Reduced Oxygen Sensitivity. *Energy Environ. Sci* **2018**, *11*, 394-406.

(7) Paetzold, U. W.; Jaysankar, M.; Gehlhaar, R.; Ahlswede, E.; Paetel, S.; Qiu, W.; Bastos, J.; Rakocevic, L.; Richards, B. S.; Aernouts, T.; *et al.* Scalable Perovskite/CIGS Thin-Film Solar Module with Power Conversion Efficiency of 17.8%. *J. Mater. Chem. A* **2017**, *5*, 9897-9906.

(8) Sutter-Fella, C. M.; Li, Y.; Amani, M.; Ager, J. W.; Toma, F. M.; Yablonovitch, E.; Sharp, I. D.; Javey, A. High Photoluminescence Quantum Yield in Band Gap Tunable Bromide Containing Mixed Halide Perovskites. *Nano Lett.*. **2016**, *16*, 800-806.

(9) Deschler, F.; Price, M.; Pathak, S.; Klintberg, L. E.; Jarausch, D.-D.; Higler, R.; Hüttner, S.; Leijtens, T.; Stranks, S. D.; Snaith, H. J.; *et al.* High Photoluminescence Efficiency and Optically Pumped Lasing in Solution-Processed Mixed Halide Perovskite Semiconductors. *J. Phys. Chem. Lett.* **2014**, *5*, 1421-1426.

(10) Cho, H.; Jeong, S.-H.; Park, M.-H.; Kim, Y.-H.; Wolf, C.; Lee, C.-L.; Heo, J. H.; Sadhanala, A.; Myoung, N.; Yoo, S.; *et al.* Overcoming the Electroluminescence Efficiency Limitations of Perovskite Light-Emitting Diodes. *Science* **2015**, *350*, 1222-1225.

(11) Aygüler, M. F.; Puscher, B. M. D.; Tong, Y.; Bein, T.; Urban, A. S.; Costa, R. D.; Docampo, P. Light-Emitting Electrochemical Cells Based on Inorganic Metal Halide Perovskite Nanocrystals. *J. Phys. D.: Appl. Phys.* **2018**, *51*, 334001.

(12) Jia, Y.; Kerner, R. A.; Grede, A. J.; Rand, B. P.; Giebink, N. C. Continuous-Wave Lasing in an Organic–inorganic Lead Halide Perovskite Semiconductor. *Nat. Photon.* **2017**, *11*, 784-788.

(13) Brenner, P.; Stulz, M.; Kapp, D.; Abzieher, T.; Paetzold, U. W.; Quintilla, A.; Howard, I. A.; Kalt, H.; Lemmer, U. Highly Stable Solution Processed Metal-Halide Perovskite Lasers on Nanoimprinted Distributed Feedback Structures. *Appl. Phys. Lett.* **2016**, *109*, 141106.

(14) Grancini, G.; Roldán-Carmona, C.; Zimmermann, I.; Mosconi, E.; Lee, X.; Martineau, D.; Narbey, S.; Oswald, F.; De Angelis, F.; Grätzel, M.; *et al.* One-Year Stable Perovskite Solar Cells by 2D/3D Interface Engineering. *Nat. Comm.* **2017**, *8*, 15684.

(15) Bush, K. A.; Palmstrom, A. F.; Yu, Z. J.; Boccard, M.; Cheacharoen, R.; Mailoa, J. P.; McMeekin, D. P.; Hoye, R. L. Z.; Bailie, C. D.; Leijtens, T.; *et al.* 23.6%-Efficient Monolithic Perovskite/Silicon Tandem Solar Cells with Improved Stability. *Nat. Energy* **2017**, *2*, 17009.

(16) Noh, J. H.; Im, S. H.; Heo, J. H.; Mandal, T. N.; Seok, S. I. Chemical Management for Colorful, Efficient, and Stable Inorganic–Organic Hybrid Nanostructured Solar Cells. *Nano Lett.*. **2013**, *13*, 1764-1769.

(17) Hoke, E. T.; Slotcavage, D. J.; Dohner, E. R.; Bowring, A. R.; Karunadasa, H. I.; McGehee, M. D. Reversible Photo-Induced Trap Formation in Mixed-Halide Hybrid Perovskites for Photovoltaics. *Chem. Sci.* **2015**, *6*, 613-617.

(18) Samu, G. F.; Janáky, C.; Kamat, P. V. A Victim of Halide Ion Segregation. How Light Soaking Affects Solar Cell Performance of Mixed Halide Lead Perovskites. *ACS Energy Lett.* **2017**, 2, 1860-1861.

(19) Slotcavage, D. J.; Karunadasa, H. I.; McGehee, M. D. Light-Induced Phase Segregation in Halide-Perovskite Absorbers. *ACS Energy Lett.* **2016**, *1*, 1199-1205.

(20) Rehman, W.; McMeekin, D. P.; Patel, J. B.; Milot, R. L.; Johnston, M. B.; Snaith, H. J.; Herz, L. M. Photovoltaic Mixed-Cation Lead Mixed-Halide Perovskites: Links Between Crystallinity, Photo-Stability and Electronic Properties. *Energy Environ. Sci.* **2017**, *10*, 361-369.

(21) Bush, K. A.; Frohna, K.; Prasanna, R.; Beal, R. E.; Leijtens, T.; Swifter, S. A.; McGehee, M. D. Compositional Engineering for Efficient Wide Band Gap Perovskites with Improved Stability to Photoinduced Phase Segregation. *ACS Energy Lett.* **2018**, *3*, 428-435.

(22) Pollak, F.H., Modulation Spectroscopy of Semiconductor and Semiconductor Microstructures. In *Handbook on Semiconductors*; M. Balkanski, Ed.; Vol.2 Optical Properties of Semiconductors; North Holland: Amsterdam, **1994**, pp 542-545.

(23) Aspnes, D. E. Third-Derivative Modulation Spectroscopy with Low-Field Electroreflectance. *Surf. Sci.* **1973**, *37*, 418-442.

(24) Huber, C.; Krämmer, C.; Sperber, D.; Magin, A.; Kalt, H.; Hetterich, M. Electroreflectance of Thin-Film Solar Cells: Simulation and Experiment. *Phys. Rev. B* **2015**, *92*, 075201.

(25) Krämmer, C.; Huber, C.; Redinger, A.; Sperber, D.; Rey, G.; Siebentritt, S.; Kalt, H.; Hetterich, M. Diffuse Electroreflectance of Thin-Film Solar Cells: Suppression of Interference-Related Lineshape Distortions. *Appl. Phys. Lett.* **2015**, *107*, 222104.

(26) Ziffer, M. E.; Mohammed, J. C.; Ginger, D. S. Electroabsorption Spectroscopy Measurements of the Exciton Binding Energy, Electron–Hole Reduced Effective Mass, and Band Gap in the Perovskite $CH_3NH_3PbI_3$. *ACS Photonics.* **2016**, *3*, 1060-1068.

(27) Wu, X.; Yu, H.; Li, N.; Wang, F.; Xu, H.; Zhao, N. Composition-Dependent Light-Induced Dipole Moment Change in Organometal Halide Perovskites. *J. Phys. Chem. C* **2015**, *119*, 1253-1259.

(28) Ruf, F.; Magin, A.; Schultes, M.; Ahlswede, E.; Kalt, H.; Hetterich, M. Excitonic Nature of Optical Transitions in Electroabsorption Spectra of Perovskite Solar Cells. *Appl. Phys. Lett.* **2018**, *112*, 083902.

(29) Shanabrook, V.; Glembocki, O. J.; Beard, W. T. Photoreflectance Modulation Mechanisms in GaAs-$Al_xGa_{1-x}As$ Multiple Quantum Wells. *Phys. Rev. B* **1987**, *35*, 2540.

(30) Pollak F. H.; Glembocki, O. J. Modulation Spectroscopy of Semiconductor Microstructures: An Overview. *Proc. SPIE* **1988**, *0946*, 2.

(31) Galluppi, M.; Geelhaar, L.; Riechert, H.; Hetterich, M.; Grau, A.; Birner, S.; Stolz, W. Bound-to-Bound and Bound-to-Free Transitions in Surface Photovoltage Spectra: Determination of the Band Offsets for $In_xGa_{1-x}As$ and $In_xGa_{1-x}As_{1-y}N_y$ Quantum Wells *Phys. Rev. B* **2005**, *72*, 155324.

(32) Hosea, T. J. C. Estimating Critical- Point Parameters from Kramers- Kronig Transformations of Modulated Reflectance Spectra. *Phys. Status Solidi B* **1995**, *189*, K43-K47.

(33) Grau, A.; Passow, T.; Hetterich, M. Temperature Dependence of the GaAsN Conduction Band Structure. *Appl. Phys. Lett.* **2006**, *89*, 202105.

(34) Hu, Y.; Aygüler, M. F.; Petrus, M. L.; Bein, T.; Docampo, P. Impact of Rubidium and Cesium Cations on the Moisture Stability of Multiple-Cation Mixed-Halide Perovskites. *ACS Energy Lett.* **2017**, *2*, 2212-2218.

(35) Puscher, B. M. D.; Aygüler, M. F.; Docampo, P.; Costa, R. D. Unveiling the Dynamic Processes in Hybrid Lead Bromide Perovskite Nanoparticle Thin Film Devices. *Adv. Energy Mater.* **2017**, *7*, 1602283.

(36) Brivio, F.; Caetano, C.; Walsh, A. Thermodynamic Origin of Photoinstability in the $CH_3NH_3Pb(I_{1-x}Br_x)_3$ Hybrid Halide Perovskite Alloy. *J. Phys. Chem. Lett.* **2016**, *7*, 1083-1087.

(37) Bischak, C. G.; Hetherington, C. L.; Wu, H.; Aloni, S.; Ogletree, D. F.; Limmer, D. T.; Ginsberg, N. S. Origin of Reversible Photoinduced Phase Separation in Hybrid Perovskites. *Nano Lett.* **2017**, *17*, 1028-1033.

(38) Yoon, S. J.; Kuno, M.; Kamat, P. V. Shift Happens. How Halide Ion Defects Influence Photoinduced Segregation in Mixed Halide Perovskites. *ACS Energy Lett.* **2017**, *2*, 1507-1514.

(39) Barker, A. J.; Sadhanala, A.; Deschler, F.; Gandini, M.; Senanayak, S. P.; Pearce, P. M.; Mosconi, E.; Pearson, A. J.; Wu, Y.; Kandada, A. R. S.; *et al.* Defect-Assisted Photoinduced Halide Segregation in Mixed-Halide Perovskite Thin Films. *ACS Energy Lett.* **2017**, *2*, 1416-1424.

(40) Howard, J. M.; Tennyson, E. M.; Barik, S.; Szostak, R.; Waks, E.; Toney, M. F.; Nogueira, A. F.; Neves, B. R. A.; Leite, M. S. Humidity-Induced Photoluminescence Hysteresis in Variable Cs/Br Ratio Hybrid Perovskites. *J. Phys. Chem. Lett.* **2018**, *9*, 3463-3469.

(41) Jong, U.-G.; Yu, C.-J.; Ri, G.-C.; McMahon, A. P.; Harrison, N. M.; Barnes, P. R. F.; Walsh, A. Influence of Water Intercalation and Hydration on Chemical Decomposition and Ion Transport in Methylammonium Lead Halide Perovskites. *J. Mater. Chem. A* **2018**, *6*, 1067-1074.

(42) Leguy, A. M. A.; Hu, Y.; Campoy-Quiles, M.; Alonso, M. I.; Weber, O. J.; Azarhoosh, P.; van Schilfgaarde, M.; Weller, M. T.; Bein, T.; Nelson, J.; *et al.* Reversible Hydration of $CH_3NH_3PbI_3$ in Films, Single Crystals, and Solar Cells. *Chem. Mater.* **2015**, *27*, 3397-3407.

(43) Aristidou, N.; Sanchez-Molina, I.; Chotchuangchutchaval, T.; Brown, M.; Martinez, L.; Rath, T.; Haque, S. A. The Role of Oxygen in the Degradation of Methylammonium Lead Trihalide Perovskite Photoactive Layers. *Angew. Chem.* **2015**, *127*, 8326-8330.

(44) Aristidou, N.; Eames, C.; Sanchez-Molina, I.; Bu, X.; Kosco, J.; Islam, M. S.; Haque, S. A. Fast Oxygen Diffusion and Iodide Defects Mediate Oxygen-Induced Degradation of Perovskite Solar Cells. *Nat. Commun.* **2016**, *8*, 15218.